JSST
Journal of Space Science & Technology

Vol. 7/ No. 1/ Spring 2014
pp. 41-48

Approximate Viscous Shock-Layer Analysis of Axisymmetric Bodies in Perfect Gas Hypersonic Flow

S. Ghasemloo[1] and S. Noori[2*]

1. Space Research Institute, Malek-e AshtarUniversity

2. Department of Aerospace Engineering, Amirkabir University of Technology,

[*]Postal Code: 158754413,Tehran, IRAN

S_noori@aut.ac.ir

In this paper, an approximate axisymmetric method is developed which can reliably calculate fully viscous hypersonic flow over blunt-nosed bodies. In this method, a Maslen's second-order pressure expression is used instead of the normal momentum equation. The combination of Maslen's second-order pressure expression and viscous shock layer equations is developed to accurately and efficiently compute hypersonic flow fields of perfect gas around blunt-body configurations. The results show that, this combination leads to more accurate solutions and less extensive computer run times in the preliminary design environment. Furthermore, the utility of Cebeci-Smith turbulence model is adequate for application to long slender bodies. The results of these computations are found to be in good agreement with available numerical and experimental data.

Keywords: Approximate, Aerodynamic Heating, HypersonicFlow, Perfect Gas

Nomenclature

h	static enthalpy, h^*/V_∞^2
h_1, h	metrics
M	Mach number
R_n	body nose radius
r	radius measured from axis of symmetry, r^*/R_n^*
s	coordinate measured along the shock wave, s^*/R_n^*
T	temperature, $T^*C_{P\infty}^*/V_\infty^2$
y	distance normal to body
ρ	density, ρ^*/ρ_∞
u	velocity component tangent to the shock, u^*/V_∞^*
v	velocity component normal to the shock, v^*/V_∞^*
ε	Reynolds number parameter, $(\mu_{ref}/\rho_\infty^* u_n^* R_n^*)^{1/2}$
Γ_b	body angle
η_n	normalized n coordinate, $1-n/n_b$
μ	viscosity, u^*/μ_{ref}^*
ξ	normalized s coordinate, $\xi = s$
w	wall value
∞	free stream condition
*	dimensional quantities

Introduction

There is a continued interest in developing improved engineering methods, thus by using the approached introduced in the presentwork forthe preliminary design, extensive computer run times can be avoided. The approximate viscous shock layer (VSL) equations have been generallyappliedto predict the flow field and convective heat flux over hypersonic reentry vehicles. The VSL equations are obtained from the full Navier-Stockes equations by keeping both viscous and inviscid terms up to the second order of the inverse square root of the Reynolds number. The VSL equations are of mixed hyperbolic-elliptic type in the subsonic nose region of a blunt body and are of mixed hyperbolic-parabolic type in the supersonic region [1]. The approximate VSL solver requires less computing time than the fullVSL solvers[2]. Therefore, an approximate method is required for solving VSL equations to provide quick and less expensive engineering estimates. Grantz et al. [3] developed an approximate axisymmetric VSL approachwhich was faster than full VSL methods. However, their method

1. Assistant Professor
2. Assistant Professor (Corresponding Author)

Recived: 2011.11.13 , Accepted: 2014.03.03

had three disadvantages: (1) too many iterations were required for the shock shape convergence,(2) the solution was inconsistent near the stagnation line, and (3) the node spacing across the shock layer was the source of oscillations in the profiles of shock layer properties.

In addition, this method did not reduce the CPU requirements as compared with the full VSL equations. Thus, there exists a need for different approximate VSL approaches to bediscovered.In the previous methods, an initial shock shape was required to start the solution of VSL equations. This was obtained by various procedures (thin viscous shock layer, inviscid solution,…),each requiring considerable computational effort. Moreover, the shock shape extending to the entire length of the body is globally iterated. The initial shock shape generation and the global iterations over the entire length of the body required considerable computational effort and run time, respectively. In this method shock shape is determined using Riley and DeJarnette algorithms [4,5] which are 3 to 5 times faster than full viscous shock layer methods [6].The present approach generates its own shock shape as a part of solution and provides a smooth shock shape in subsonic and supersonic regions. Therefore, the input shock shape obtained from a different solution is not required. This approacheliminates the need for initial shock shape, which was required by previous methods of solution. Moreover, the global iterations are limited to the subsonic region which is a small region in the hypersonic flow over the blunt bodies. The VSL equations are solved in a shock oriented (rather than the traditional body oriented) coordinate system. Note that the use of a body coordinate system introduces discontinuities in the solution of governing equations associated with the surface curvature discontinuity, such as at the sphere–cone tangency point of a spherically blunted cone. This method is an excellent tool for parametric study and preliminary design of hypersonic vehicles and provides a computational capability which reduces the CPU times and expands the range of application for the prediction of hypersonic heating rates.The above-mentioned disadvantages of Grantz's method were resolved by this method. The accuracy of the developed code is validated by comparing the computational results with other solutions and available experimental data.

Governing Equations

The Viscous Shock Layer equations written in curvilinear coordinates for axisymmetric flow are presented below. In this work, these equations are written in a nondimensional form:

Continuity:

$$\frac{\partial}{\partial s}(\rho u h_3)+\frac{\partial}{\partial n}(\rho v h_1 h_3)=0 \tag{1}$$

N-momentum:

$$\rho\left(\frac{u}{h_1}\frac{\partial v}{\partial s}+v\frac{\partial v}{\partial n}-\frac{u^2}{h_1}\frac{\partial h_1}{\partial n}\right)+\frac{\partial p}{\partial n}=0 \tag{2}$$

S-momentum:

$$\rho\left(\frac{u}{h_1}\frac{\partial u}{\partial s}+v\frac{\partial u}{\partial n}+\frac{uv}{h_1}\frac{\partial h_1}{\partial n}\right)+\frac{1}{h_1}\frac{\partial p}{\partial s}= \varepsilon^2\left\{\frac{\partial}{\partial n}\left[\mu\left(\frac{\partial u}{\partial n}-\frac{u}{h_1}\frac{\partial h_1}{\partial n}\right)\right]+\mu\left(\frac{2}{h_1}\frac{\partial h_1}{\partial n}+\frac{1}{h_3}\frac{\partial h_3}{\partial n}\right)\left(\frac{\partial u}{\partial n}-\frac{u}{h_1}\frac{\partial h_1}{\partial n}\right)\right\} \tag{3}$$

Energy:

$$\rho\left(\frac{u}{h_1}\frac{\partial h}{\partial s}+v\frac{\partial h}{\partial n}\right)-\frac{u}{h_1}\frac{\partial p}{\partial s}-v\frac{\partial p}{\partial n}= \varepsilon^2\left\{\frac{\partial}{\partial n}\left(\frac{\mu}{\mathrm{Pr}}\frac{\partial h}{\partial n}\right)+\frac{\mu}{\mathrm{Pr}}\frac{\partial h}{\partial n}\left(\frac{1}{h_1}\frac{\partial h_1}{\partial n}+\frac{1}{h_3}\frac{\partial h_3}{\partial n}\right)+ +\mu\left(h_1\frac{\partial u}{\partial n}-u\frac{\partial h_1}{\partial n}\right)\left(\frac{1}{h_1}\frac{\partial u}{\partial n}-\frac{u}{h_1^2}\frac{\partial h_1}{\partial n}\right)\right\} \tag{4}$$

Where u and v are velocity components, h_1 and h_3 are Metrics (shape factor) and ε is Reynold's number that:

$$h_1=1-nk_s \quad , \quad h_3=r_s-n.\cos\alpha \tag{5}$$

$$\varepsilon^2=\frac{\mu^*_{ref}}{\rho^*_\infty u^*_\infty R^*_n} \tag{6}$$

In the above equation R_n is nose radius of curvature. The superscript of * shows the dimensional values. These equations could be transformed to either a body-normal or a shock-normal system. Here, we have a shock-normal system. The shock-oriented coordinate system is shown in Figure 1. The governing equations are transformed from (s,n) to a new computational coordinate system of (ξ,η_n), where:

$$\xi=s \quad , \quad \eta_n=1-\frac{n}{n_b} \tag{7}$$

Energy and S-momentum equations can be written as:

$$A_0\frac{\partial^2 W}{\partial\eta_n^2}+A_1\frac{\partial W}{\partial\eta_n}+A_2W+A_3+A_4\frac{\partial W}{\partial\xi}=0 \tag{8}$$

Where w represents the dependent variables of u (velocity components) and h (enthalpy) for momentum equations and energy equation, respectively. Also, by using the Cebeci-Smith turbulence model [7] in this study, its coefficient would be $\varepsilon^+=\frac{\mu_t}{\mu}$, and the

coefficients for above equations with turbulence coefficient are:

ξ-momentum :

$$\rho\left(\frac{u}{h_1}\left[\frac{\partial u}{\partial \xi}-\frac{\eta_n-1}{n_b}\frac{dn_b}{d\xi}\frac{\partial u}{\partial \eta_n}\right]-\frac{v}{n_b}\left[\frac{\partial u}{\partial \eta_n}+\frac{u}{h_1}\frac{\partial h_1}{\partial \eta_n}\right]\right)$$
$$+\frac{1}{h_1}\left[\frac{\partial p}{\partial \xi}-\frac{\eta_n-1}{n_b}\frac{dn_b}{d\xi}\frac{\partial p}{\partial \eta_n}\right]$$
$$=\frac{\varepsilon^2}{n_b^2}\left(\frac{\partial}{\partial \eta_n}\left[\mu\left(1+\varepsilon^+\right)\frac{\partial u}{\partial \eta_n}-\mu\frac{u}{h_1}\frac{\partial h_1}{\partial \eta_n}\right]\right) \quad (9)$$
$$\frac{\varepsilon^2}{n_b^2}\left(\left(\frac{2}{h_1}\frac{\partial h_1}{\partial \eta_n}+\frac{1}{h_3}\frac{\partial h_3}{\partial \eta_n}\right)+\left[\mu\left(1+\varepsilon^+\right)\frac{\partial u}{\partial \eta_n}-\mu\frac{u}{h_1}\frac{\partial h_1}{\partial \eta_n}\right]\right)$$

Energy:

$$\rho\left(\frac{u}{h_1}\left[\frac{\partial h}{\partial \xi}-\frac{\eta_n-1}{n_b}\frac{dn_b}{d\xi}\frac{\partial h}{\partial \eta_n}\right]-\frac{v}{n_b}\frac{\partial h}{\partial \eta_n}\right)-\frac{u}{h_1}\left[\frac{\partial p}{\partial \xi}-\frac{\eta_n-1}{n_b}\frac{dn_b}{d\xi}\frac{\partial p}{\partial \eta_n}\right]+$$
$$+\frac{v}{n_b}\frac{\partial p}{\partial \eta_n}=\frac{\epsilon^2}{n_b^2}\left(\frac{\partial}{\partial \eta_n}\left[\frac{\mu}{\mathrm{Pr}}\left(1+\varepsilon^+\frac{\mathrm{Pr}}{\mathrm{Pr}_t}\right)\frac{\partial h}{\partial \eta_n}\right]\right)+$$
$$\frac{\varepsilon^2}{n_b^2}\left(\frac{\mu}{\mathrm{Pr}}\left(1+\varepsilon^+\frac{\mathrm{Pr}}{\mathrm{Pr}_t}\right)\frac{\partial h}{\partial \eta_n}\left(\frac{1}{h_1}\frac{\partial h_1}{\partial \eta_n}+\frac{1}{h_3}\frac{\partial h_3}{\partial \eta_n}\right)\right)+ \quad (10)$$
$$\frac{\varepsilon^2}{n_b^2}\left(\left[\mu\left(1+\varepsilon^+\right)\left\{\left(\frac{\partial u}{\partial \eta_n}\right)^2-\frac{2u}{h_1}\frac{\partial h_1}{\partial \eta_n}\frac{\partial h}{\partial \eta_n}\right\}+\mu\left(\frac{u}{h_1}\frac{\partial h_1}{\partial \eta_n}\right)^2\right]\right)$$

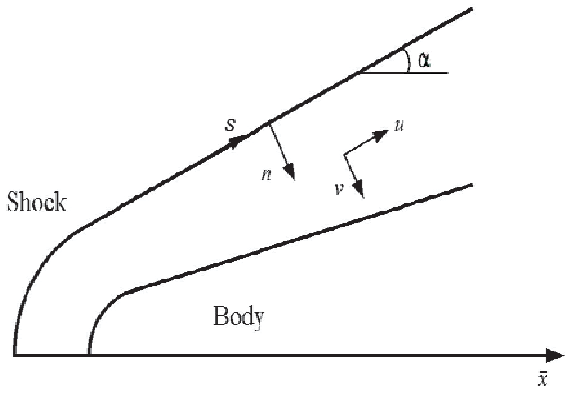

Fig. 1 Shock-oriented coordinate system

Where subscript s identifies shock value. In this approach, Maslen's second order pressure equation is used instead of the normal momentum equation:

$$P=P_s+\frac{k_s r_s u_s}{2}(\eta-1)-\frac{v_s\sin\alpha}{4}\left(1+\frac{k_s r_s}{\cos\alpha}\right)\left(\eta^2-1\right) \quad (10)$$

Where

$$\eta=\frac{\psi}{\psi_s} \quad (11)$$

Also, the shock layer thickness is calculated by:

$$\left[2\cos\alpha\int_0^1 \rho u(\eta_n-1)d\eta_n\right]n_b^2$$
$$+\left[2r_s\int_0^1 \rho u d\eta_n\right]n_b-r_s^2=0 \quad (12)$$

The above set of equationsaresupplemented by the equation of state.

Stagnation Line

The stagnation line is a singularity in the standard VSL equations. This singularity is handled by representing the dependent variables on the stagnation line with a truncated power series. In the shock-oriented system, an explicit limiting form of the governing equations as $\xi\to 0$ can be calculated [8] since Maslen's relation provides analytic derivatives of the pressure. Thus, a set of ordinary differential equations which areconsistent with the general governing equations can be obtained.

Shock shape

In the present approach, the shock shape is generated as part of the solution. The shock shape is calculated using the method which is presented in Ref. 4. As mentioned earlier, the subsonic-transonic region is elliptic in nature, therefore, a marching scheme is not well posed. Thus, the complete shock shape for the entire subsonic-transonic region must be determined iteratively. A marching procedure is then used downstream of the subsonic-transonic region where the inviscid layer is supersonic. Generally, the three-dimensional shock surface in the subsonic-transonic region can be represented by three longitudinal conic sections blended in the circumferential direction with an ellipse as:

$$r=f(x,\phi) \quad (13)$$

Where (x,r,ϕ) are cylindrical coordinates. The x axis is aligned with the freestream velocity vector. Also f(x,ϕ) is defined as:

$$f^2\left[B(x)\cos^2(\phi)+\sin^2(\phi)\right]+fC(x)\cos(\phi)=D(x) \quad (14)$$

in which

$$B(x)=\frac{f_2^2}{f_1 f_3}\ ;\ C(x)=B(x)(f_3-f_1)\ ;\ D(x)=f_2^2 \quad (15)$$

Note that f(x,ϕ) is the radial coordinate of the 3D shock surface in a shock cylindrical coordinate system. The equation of the longitudinal conic sections is given by

$$f_k^2+b_k x^2-2c_k x+2d_k x f_k=0\ ,k=1,2,3 \quad (16)$$

Where k represents shock profiles for ϕ=0°, 90° and 180°, respectively. The shock shape defined above, includes nine parameters of bk, ck and dk where k=1,2,3. For an axisymmetric flow, the total number of parameters governing the shock surface is reduced to b1 and c1. The global iteration of the shock surface in the subsonic region involves matching the shape computed from the VSL equations with the actual body geometry. To insure a good starting solution for the downstream marching procedure, the

matching body points are located at the end of the subsonic region where the inviscid layer is supersonic. Note that in this procedure flowfield is also solved behind the shock wave. First, initial values are guessed for the above two parameters. The appropriate initial shock shape is produced by the values of 0.98 and 1.2 for b1 and c1. Since the initial shock shape (and the resulting jump condition) is known, the governing equations can be solved for the entire subsonic region to obtain the calculated shock layer thickness, n_b, for all stations. Next the calculated thickness can be determined from the continuity equation:

$$\left(\frac{\cos\Gamma_s}{r_s^2}\int_0^1 \rho u(\eta_n - 1)d\eta_n\right)n_b^2 + \left(\frac{1}{r_s}\int_0^1 \rho u d\eta_n\right)n_b - \frac{1}{2} = 0 \qquad (17)$$

The values for the calculated shock layer thickness at the two stations near the end of the subsonic region are compared with the values dictated by the geometry. Based on the calculated and the geometric shock layer thickness, new values of shock shape parameters b1 and c1 are computed. With each variation of these two parameters, the flowfield is solved for the entire subsonic region. This procedure is repeated until the calculated values of n_b at these two stations match the geometric values. Downstream of this region, the shock shape is calculated through a marching scheme requiring no global iterations. For the supersonic region, the shock shape at the current station is described by a truncated Taylor's series [5] .

$$r_s = r_{si-1} + \Delta x_s\left(\frac{dr_s}{dx_s}\right)_{i-1} + \frac{\Delta x_s^2}{6}\left[2\left(\frac{d^2 r_s}{dx_s^2}\right)_{i-1} + \left(\frac{d^2 r_s}{dx_s^2}\right)_i\right] \qquad (18)$$

Where the shock slope is given by

$$\frac{dr_s}{dx_s} = \left(\frac{dr_s}{dx_s}\right)_{i-1} + \frac{\Delta x_s}{2}\left[\left(\frac{d^2 r_s}{dx_s^2}\right)_{i-1} + \left(\frac{d^2 r_s}{dx_s^2}\right)_i\right] \qquad (19)$$

In these equations, the only unknown is the second derivative of r_s with respect to x_s (which is proportional to the shock curvature) at the current station. The initial value for this parameter is calculated by linear extrapolation of its values at the previous two stations. Once the shock geometry and the corresponding jump conditions are constrained, the governing equations are solved. Then the calculated and the geometric values of n_b are compared to determine anerror (δerr). Through successive application of the secant method (accompanied by a solution to the fluid equations), δerr converges to a specified tolerance (1×10^{-4}). In summary, in the subsonic-transonic region, shock shape is specified usingan algebraic relation and is corrected through global iterations throughout that region. The shock shape is computed as part of the solution beyond the subsonic-transonic region. Thus, the shock shape is not required as an input by the user.

Method of Solution

For the solution of governing equations, the shock shape should be guessed. In this work, for stagnation line, in the subsonic or supersonic regions, the shock shape is calculated from the approximate method of Riley and DeJarnette. Since the shock shape is known, the approximate viscous shock layer equations can be solved in the shock layer along a line normal to the shock surface. The governing equations are solved along the stagnation line and then marched downstream and around the body. In each marching step the pressure is calculated from Maslen's relation in the shock layer, then the streamwise momentum and energy equations (for determining u, h) are solved using a fully implicit method in the shock layer. Density is calculated from the equation of state. Finally the normal component of velocity is determined by the solution of continuity equation. Since the subsonic-transonic region is elliptic in nature, this portion of the flowfield must be solved in a global fashion. Aft of the subsonic-transonic region, since the inviscid layer is supersonic,a marching technique is employed.For this region, the shock shape at the current station is extrapolated from the previous station.

The finite-difference representations are substituted for the partial derivatives. In this study, for an arbitrary point *j* at station *k:*

$$\frac{\partial^2 W}{\partial \eta_n^2} = \frac{2\left[W_{i,j+1} - (1+\beta)W_{i,j} + \beta W_{i,j-1}\right]}{\Delta\eta_{n_{j+1}}^2 + \beta\Delta\eta_{n_j}^2}$$
$$\frac{\partial W}{\partial \eta_n} = \frac{W_{i,j+1} - (1-\beta^2)W_{i,j} - \beta^2 W_{i,j-1}}{\Delta\eta_{n_{j+1}} + \beta^2\Delta\eta_{n_j}} \qquad (20)$$
$$\frac{\partial W}{\partial \xi} = \frac{W_{i,j} - W_{i-1,j}}{\Delta\xi_i}$$

Where

$$\Delta\eta_{n_j} = \eta_{n_j} - \eta_{n_{j-1}}$$
$$\beta = \frac{\Delta\eta_{n_{j+1}}}{\Delta\eta_{n_j}} \qquad (21)$$
$$\Delta\xi_i = \xi_i - \xi_{i-1}$$

Therefore, the finite differenced equations are written again asbelow:

$$A_j W_{i,j-1} + B_j W_{i,j} + C_i W_{i,j+1} = D_j \qquad (22)$$

Where

$$
\begin{aligned}
A_i &= \alpha_1\beta A_0 - \alpha_2\beta^2 A_1 \\
B_i &= -\alpha_1(1+\beta)A_0 - \alpha_2(1-\beta^2)A_1 + A_2 + \frac{A_4}{\Delta\xi_i} \\
C_i &= \alpha_1 A_0 + \alpha_2 A_1 \\
D_i &= -A_3 + \frac{W_{i-1,j}}{\Delta\xi_i}A_4
\end{aligned}
\qquad (23)
$$

$$
\alpha_1 = \frac{2}{\Delta\eta_{n_{j+1}}^2 + \beta\Delta\eta_{n_j}^2} \quad \alpha_2 = \frac{1}{\Delta\eta_{n_{j+1}} + \beta^2\Delta\eta_{n_j}} \quad \beta = \frac{\Delta\eta_{n_{j+1}}}{\Delta\eta_{n_j}}
$$

By using these equations, the shock layer properties are obtained.

Results

The following section demonstratescomparisons of the predicted wall heat-transfer distribution with the available experimental data [9]. The algorithms employed here are fully-implicit. The case examined is flow over a 5 deg half-angle spherically blunted cone at zero angle of attack. The free stream conditions are M_∞= 15, T_∞=266 k and ρ_∞=0.001788 Kg/m3. The wall temperature is T_w=1256 k. also, R_{nose}=0.0381 m.

Figures 2 and 3 show the heating rate for R_{nose}=0.0381 m. These figures, illustrate the laminar flow and Turbulence flow, respectively. Good agreement can be observed between the results of present method and experimental data. The negligible difference between these results is due to using an approximate VSL equation. It is believed that Maslen's pressure relation is the source of this deviation. Since this method is faster than the method of Ref. [10], it is appropriate for the preliminary design. In this figure, the maximum error of the heating rate respect to the experimental data is 6% for laminar flow and 10% for turbulence flow. In addition, Figure 4 shows the heating rate near the nose and indicates these differences clearly.

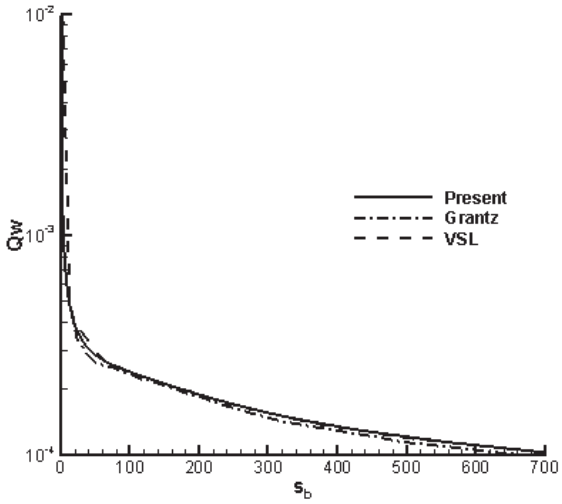

Fig.2 Heatingrate in laminar flow

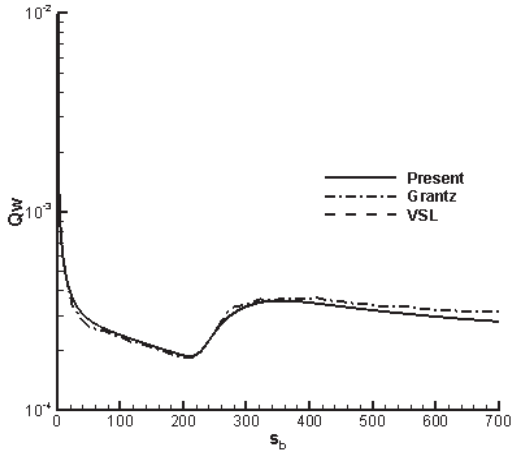

Fig.3 Heatingrate in turbulence flow

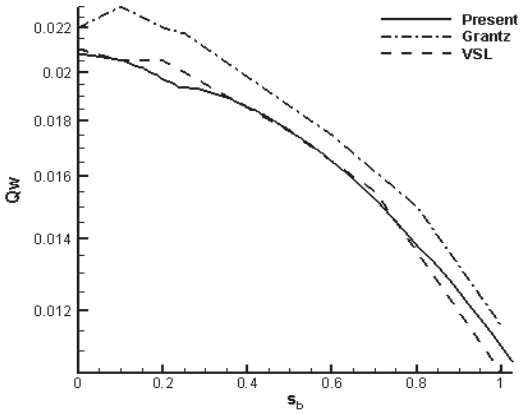

Fig.4 Heating rate near the nose

Figure 5 shows the body pressure distribution over this case. Grantz in Ref. [3] has explained that the agreement between the experimental and calculated pressure from Maslen's relation is excellent. This figure shows the error of pressure is negligible (less than 5 percent).

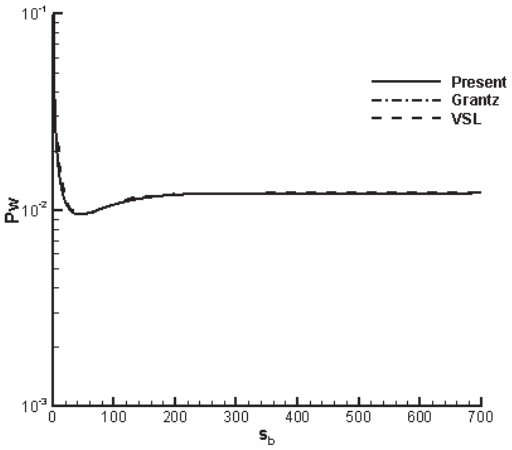

Fig.5 Pressure distribution along the body

Figure 6 indicates the pressure distribution near the nose region. Grantz's method and present method used the Maslen's expression for the calculation of pressure. The error of this figure is less than 5 percent.

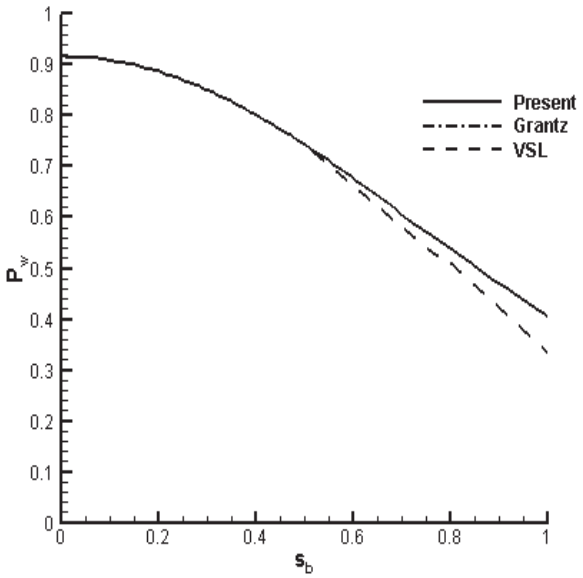

Fig. 6 Pressure distribution near the nose

In Figure 7, the shock layer is shown. The approximate techniques agree with the VSL results. However, inthe close-upgiven in Figure 8, note that the two approximate approaches yield a thinner shock layer than the VSL algorithm in the overexpansion region.

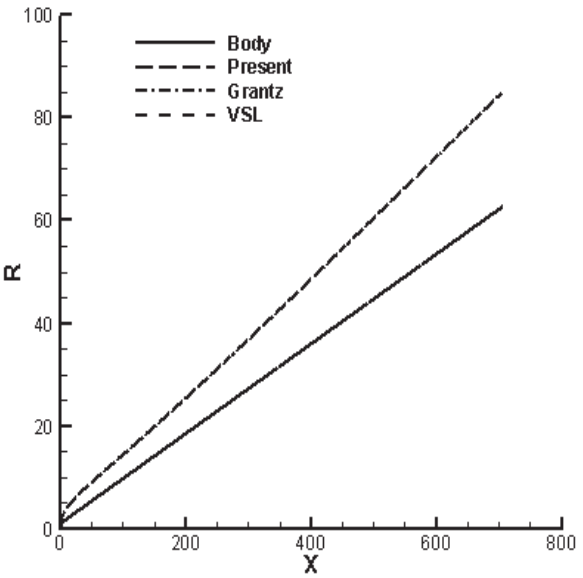

Fig.7 Shock shape along the body

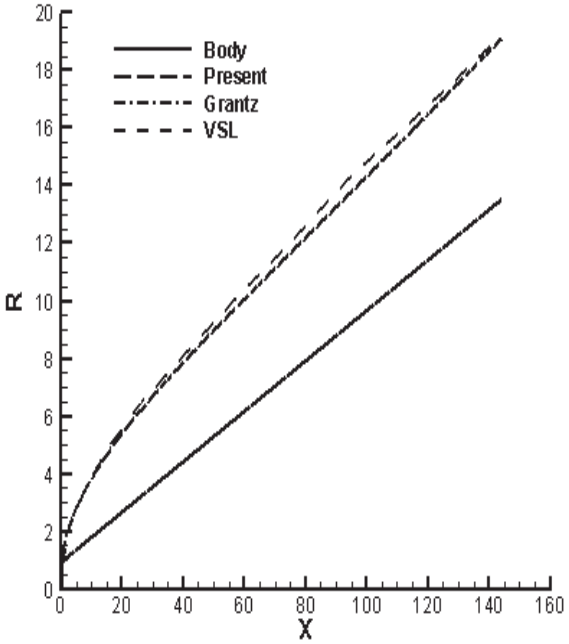

Fig.8 Shock shape near the nose (overexpansion)

Other figures provide extra information on the stagnation region results. In Figure 9, the stagnation region pressure profile for all three methods is exposed. One can conclude that there is excellent agreement between these results; i.e., about three percent. The aforementioned error is due to the utility of approximate Maslen'ssecond-order pressure expression. Density profile comparison results are presented in Figure 10.The significant error is not shown since this parameter relates the pressure and pressure expression which is approximately valid in all flowfield. As the result, good agreement for the density profile is included in those areas where the pressure profile is well-predicted. As it is evidentin Figure 11, the normalized tangent velocity profile ($\bar{u} = u/u_s$) has a smooth distribution in the stagnation region. These results are in close agreement with each other, although the VSL results are different. This difference may be due to the VSL limiting form of the streamwise momentum equation. The error of this result is roughly two percent in this region. In Figure 12, the normal velocity results of the VSL and present method are virtually identical, while the results of Ref. [11] differ from them slightly. The approximate relation for v used in Ref. [11] is the source of this difference. Figure 13 shows that the enthalpy profile of the three methods is virtually identical on the stagnation line. It is dictated by Energy equation solving. The error of this profile is about 2 percent.

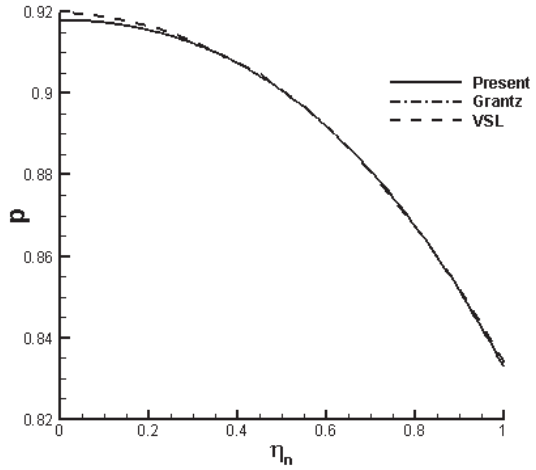

Fig.9 Pressure profile comparison in stagnation region

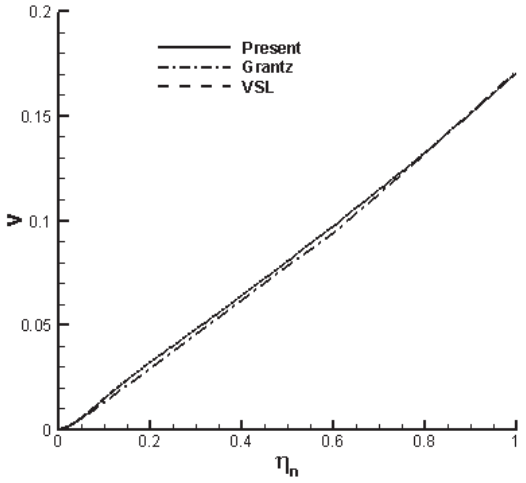

Fig. 12 Normal velocityprofile comparison in stagnation region

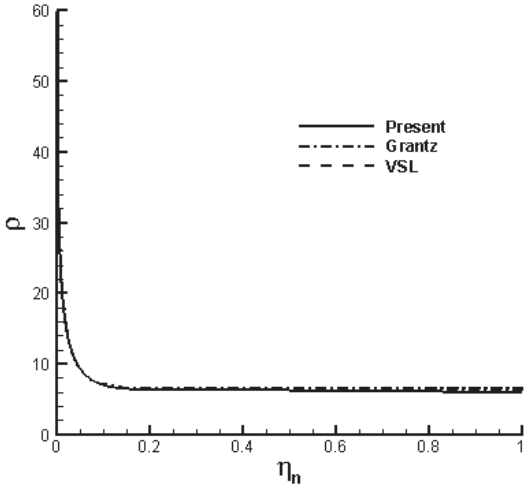

Fig.10 Density profile comparison in stagnation region

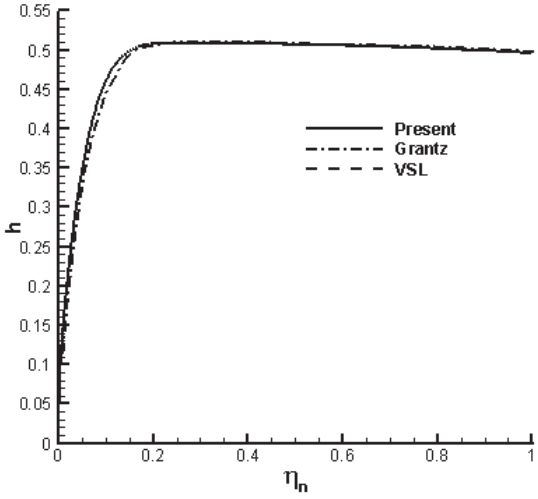

Fig. 13 Enthalpy profile comparison in stagnation region

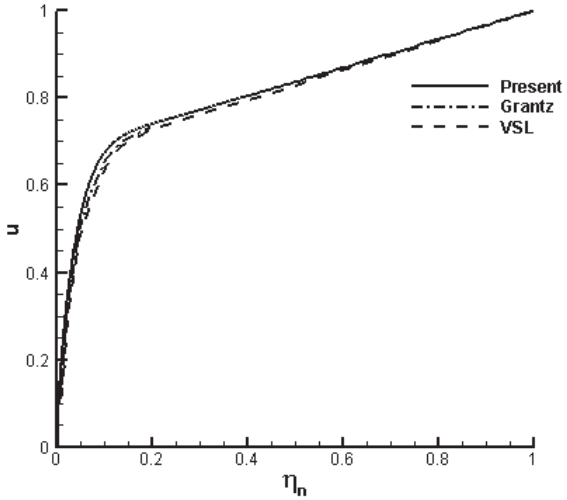

Fig. 11 Tangent velocity profile comparison in stagnation region

Conclusion

In this investigation, a method is developed to solve hypersonic flowfield about axisymmetric blunt bodies. This method, when compared to VSL solutions, is provedto be smooth and accurate for perfect gases. Moreover, governing equations are solved in a shock-oriented coordinate system. Usingthe present method the surface heating rates and flowfield properties can bepredicted faster in comparison with the other methods. Since the subsonic region is only a small portion of the flow field for hypersonic flows over slender bodies, and the global iteration is confined tothis region only in the present method, a significant reduction in CPU time is achieved. Moreover, by using the shock coordinated systems, the junction point problem in sphere-cone configurations is solved. Results of the present method

compare quite favorably with experimental data and other predictions. Furthermore, these calculations have excellent agreement between the VSL and the approximate approaches and this event is seen in the nose region specially. This method calculates their stagnation values more smoothly than the VSL solution and some approximate approaches.

References

[1] Anderson, J.D., Jr., *Hypersonic and High Temperature Gas Dynamics*', McGraw-Hill, Inc., 1989.

[2] Ghasemloo, S. and Mani, M., "Viscous Shock Layer Solution around Hypersonic Bodies for Low and High Altitude Flow," *Amirkabir Journal of Science and Technology*, Vol. 18, No. b66, 2007, pp. 81-89.

[3] Grantz, A.C., DeJarnette, F.R., Thompson, R.A., "Approximate Viscous-Shock Layer Method for Hypersonic Flows over Blunt-Nosed Bodies," *Journal of Spacecraft and Rockets*, Vol. 27, No.6, 1990, pp. 597-605.

[4] Riley, C.J., DeJarnette, F.R., "Engineering Aerodynamic Heating Method for Hypersonic Flow," *Journal of Spacecraft and Rockets*, Vol. 29, No.3, 1992, pp. 327-334.

[5] Riley, C. J., An Engineering Method for Interactive Inviscid-Boundary Layers in Three-Dimensional Hypersonic Flows, (PhD Thesis), North Carolina State University, 1992.

[6] MalekzadehDirin, M., Karimian, S.M.H., "Approximate Three-Dimensional Viscous Shock-Layer Method for Hypersonic Flow over Blunt-Nosed Bodies," *AIAA paper 03-154*, 2003.

[7] Cebeci, T. and Smith, A.M.O. "A Finite-Difference Method for Calculating Compressible Laminar and Turbulent Boundary Layers." *Journal of Basic Engineering*, 1970, pp. 523-535.

[8] Noori, S., Karimian, S.M.H. and Malekzadeh, M., "Numerical Solution of Three-Dimensional Viscous Shock Layer Using Axisymmetric Analog along the Streamlines," *International Journal of Numerical Methods for Heat & Fluid Flow*, Vol. 18, No. 1, 2008, pp. 36-49.

[9] Cleary, J.W. "Effects of Angle of Attack and Bluntness on Laminar Heating Rate Distributions on a 15 degree Cone at a Mach Number of 10.6," NASA TN 5450, 1969.

[10] Murray, A.L., and Lewis, C.H. "Hypersonic Three-Dimensional Viscous Shock Layer Flows over Blunt Bodies," *AIAA Journal*, Vol. 16, No. 12, 1978, pp. 1279-1286.

[11] Gupta, R.N., Lee, K.P., Moss, J.N., Zoby, E.V., and Tiwari, S.N. "Viscous Shock-Layer Analysis of the High-Reynolds-Number Hypersonic Flow Past Long Slender Bodies," AIAA Paper 87-2487, 1987.